ECOSYSTEMS   CrossMark

Aridity Induces Nonlinear Effects of Human Disturbance on Precipitation-Use Efficiency of Iberian Woodlands

Mariano Moreno-de las Heras,[1]* Esther Bochet,[2] Vicente Monleón,[3] Tíscar Espigares,[4] José Manuel Nicolau,[5] María José Molina,[2] and Patricio García-Fayos[2]

[1]Institute of Environmental Assessment and Water Research (IDAEA), Spanish Research Council (CSIC), Jordi Girona 18, 08034 Barcelona, Spain; [2]Desertification Research Centre (CIDE, CSIC-UV-GV), 46113 Moncada, Valencia, Spain; [3]US Forest Service Pacific Northwest Research Station, Corvallis, Oregon 97331, USA; [4]Department of Life Sciences, Faculty of Biology, Environmental Sciences and Chemistry, University of Alcalá, 28805 Alcalá de Henares, Madrid, Spain; [5]Environmental Sciences Institute, Huesca Technological College, University of Zaragoza, 22071 Huesca, Spain

ABSTRACT

The effects of ecosystem degradation are pervasive worldwide and increasingly concerning under the present context of global changes in climate and land use. Theoretical studies and empirical evidence increasingly suggest that drylands are particularly prone to develop nonlinear functional changes in response to climate variations and human disturbance. Precipitation-use efficiency (PUE) represents the ratio of vegetation production to precipitation and provides a tool for evaluating human and climate impacts on landscape functionality. Holm oak (*Quercus ilex*) woodlands are one of the most conspicuous dry forest ecosystems in the western Mediterranean basin and present a variety of degraded states, due to their long history of human use. We studied the response of Iberian holm oak woodlands to human disturbance along an aridity gradient (that is, semi-arid, dry-transition and sub-humid conditions) using PUE estimations from enhanced vegetation index (EVI) observations of the Moderate-Resolution Imaging Spectroradiometer (MODIS). Our results indicated that PUE decreased linearly with disturbance intensity in sub-humid holm oak woodlands, but showed accelerated, nonlinear reductions with increased disturbance intensity in semi-arid and dry-transition holm oak sites. The impact of disturbance on PUE was larger for dry years than for wet years, and these differences increased with aridity from sub-humid to dry-transition and semi-arid holm oak woodlands. Therefore, aridity may also interact with ecosystem degradation in holm oak woodlands by reducing the landscape ability to buffer large changes in vegetation production caused by climate variability.

Key words: ecosystem functionality changes; drylands; global change; holm oak woodlands; ecosystem degradation; land use; MODIS EVI.

INTRODUCTION

Ecosystem degradation represents a worldwide pervasive phenomenon that pertains to the loss of ecosystem function and productivity resulting from various factors, including human activities and climatic variations (Bai and others 2013). The present changes in climate and land use are affecting biodiversity and landscape functioning at an unprecedented rate, increasing global concerns about ecosystem degradation (McLean and Willson 2011; Valiente-Baunet and Verdú 2013). Drylands, which extend over 40% of the Earth's surface and support nearly 2.5 billion inhabitants, are significantly impacted by degradation (up to 20% of these lands are affected by some form of severe ecosystem degradation) and face a variety of threats associated with global environmental change (Millennium Ecosystem Assessment 2005). Sustainable dryland management, therefore, demands a sound understanding of the factors and mechanisms that regulate the responses of dryland ecosystems to human pressures and climate change (Maestre and others 2016).

How ecosystems undergo environmental change is recognized as one of the main frontiers in ecology and environmental sciences (Rietkerk and others 2004; Peters and others 2006; Berdugo and others 2017). Ecosystem degradation may take place either linearly, in a gradual way, or more abruptly, in a nonlinear manner, in response to the effects of disturbance and changes in climate (Scheffer and others 2001). Both theoretical studies and empirical evidence increasingly suggest that drylands are particularly prone to develop nonlinear changes in their structure and function in response to external stressors (Noy-Meir 1975; Scheffer and others 2001; Rietkerk and others 2004; Kéfi and others 2007; Bestelmeyer and others 2011). In these dry landscapes, where vegetation cover is typically 'patchy' or spatially heterogeneous, plant–plant positive interactions (that is, facilitation) and efficient spatial redistribution of resources (for example, water, sediments, nutrients, propagules) between bare and vegetated areas by surface runoff provide landscape stability over a range of climate and land-use conditions (Saco and Moreno-de las Heras 2013; Soliveres and others 2015; Bochet 2015; Kéfi and others 2016). However, as climate forcing or disturbance intensity increase, significant deterioration of the stabilizing ecosystem mechanisms may induce rapid, accelerated loss of ecosystem function and the alteration of landscape structure (Moreno-de las Heras and others 2012; Okin and others 2015; Xu and others 2015). The most extreme alterations may take place in the form of largely irreversible landscape changes, thus hindering the natural recovery of ecosystem function (Schlesinger and others 1990; Peters and others 2006; Mayor and others 2013; Moreno-de las Heras and others 2015; Martínez-Valderrama and others 2016).

Precipitation-use efficiency (hereafter termed PUE) represents the ratio of vegetation net primary production (NPP) to precipitation over a given period of time, typically a growing season or hydrological year (Le Houerou 1984). PUE has been widely applied for assessing the degree of degradation or loss of ecosystem function in drylands, where human disturbance of vegetation and soil conditions can induce reductions up to 20–50% on the ecosystem capacity to convert precipitation into vegetation production (Le Houerou 1984; O'Connor and others 2001; Holm and others 2003; Moreno-de las Heras and others 2012). PUE has also shown sensitivity to inter-annual variations of precipitation, reflecting the NPP dependence on climate conditions (Huxman and others 2004; Wessels and others 2007; Ponce-Campos and others 2013; Zhang and others 2014). Therefore, PUE represents an excellent evaluation tool for the assessment of human and climate impacts on landscape functionality (that is, the integrity of landscape functions, such as nutrient cycling, water budgeting and primary production) in drylands (Holm and others 2003; Verón and Paruelo 2010; Moreno-de las Heras and others 2012; Ruppert and others 2012). The availability of decadal series of remote-sensed vegetation indices that strongly correlate with NPP, such as the normalized difference and the enhanced vegetation indices (NDVI and EVI, respectively), facilitates the application of large, regional-scale PUE analysis for monitoring landscape functionality in drylands (Gaitán and others 2014; Zhang and others 2014; Martínez-Valderrama and others 2016).

Dryland ecosystems across the Mediterranean basin exhibit varying degrees of degradation due to their very long history of human use and are reported to be one of the most vulnerable landscapes in relation to future climate scenarios (Grove and Rackham 2001; García-Fayos and Bochet 2009). In the Iberian Peninsula, Martinez-Valderrama and others (2016) estimated that ecosystem degradation affects about 20% of its territory, mainly in agricultural landscapes and woodlands. Holm oak (*Quercus ilex*) woodlands are one of the most conspicuous dry forest ecosystems in the Iberian Peninsula and the western Mediterranean basin, and have been impacted by humans for at least 4
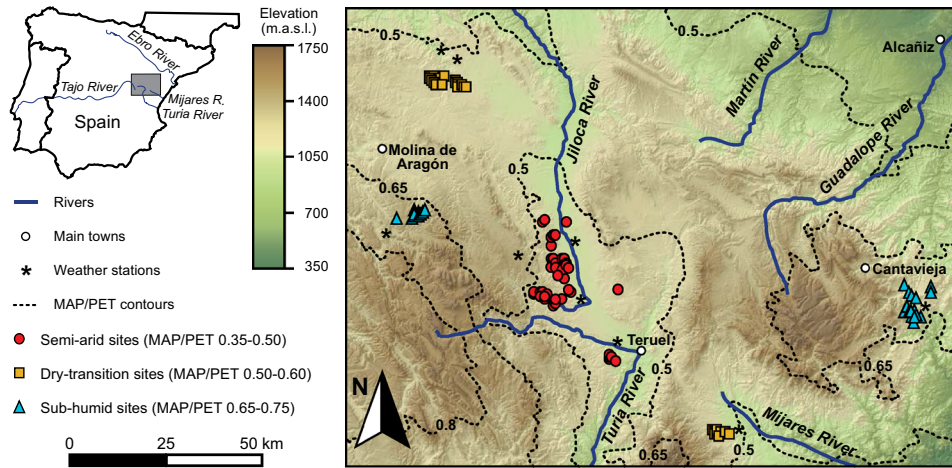
Figure 1. Location map (area is approximately 20,000 km^2). Each study site has a size of 231 × 231 m. Total number of sites is 138 (53, 51 and 34 sites for semi-arid, dry-transition and sub-humid climate conditions, respectively). Coordinates and general characteristics for both the study sites and weather stations are detailed in the electronicsupplementary material of Appendix A: Tables A1 (sites) and A2 (stations).

millennia (Terradas 1999). We studied the response of holm oak woodlands to human disturbance along an aridity gradient (that is, semi-arid, dry-transition and sub-humid conditions) across an approximately 20,000 km^2 region in eastern Spain, using remote-sensing estimations of PUE from decadal (2000–2014) EVI observations from the Moderate-Resolution Imaging Spectroradiometer (MODIS). We hypothesized that aridity largely influences the response of vegetation PUE to human disturbances, with the less arid, sub-humid extreme of the gradient showing linear reductions in landscape functionality and the semi-arid extreme showing accelerated, nonlinear reductions in the amount of vegetation production per rainfall unit. Since climate variability in drylands may interact with the effects of disturbance on ecosystem functions (Pickup 1996; Dube and Pickup 2001; Hein 2006), we also expected human disturbance to cause a stronger impact on PUE values in dry years due to unfavorable conditions for vegetation growth.

MATERIALS AND METHODS

Study Area

Our study sites are located within an extensive 20,000 km^2 region in eastern Spain, comprising areas of the basins of the Tajo, Ebro, Turia and Mijares rivers (Figure 1). The climate is Mediterranean, with two wet periods (April–June and September–November) during which more than 60% total precipitation is concentrated. Mean annual precipitation (MAP) and air temperature are

350–700 mm and 9.0–12.5°C, respectively. Potential evapotranspiration (PET) is 850–950 mm. Aridity, calculated as the ratio of MAP to PET (UNEP 1992), ranges from 0.35 to 0.85. Holm oak woodlands in the region are highly impacted by human activities due to a long history of land use, mainly fuel wood consumption, domestic livestock and agriculture (Stevenson 2000; García-Fayos and Bochet 2009).

We selected 138 study sites for analysis (each 231 × 231 m, corresponding to the pixel size of the UTM-re-projected MODIS MOD13Q1 product that was later applied for the calculation of PUE) distributed within semi-arid, dry-transition and sub-humid climate conditions with a MAP/PET ratio of 0.35–0.50 (53 sites), 0.50–0.60 (51 sites) and 0.65–0.75 (34 sites), respectively (Figure 1). Site selection was decided upon by applying GIS techniques and field validation to identify for each climate aridity level (semi-arid, dry-transition and sub-humid) a large number of representative holm oak sites in a variety of deforestation levels. All the sites were selected in areas with nearby availability of reference meteorological records (that is, daily precipitation series) and homogeneous landscape topography and lithology. Specific site selection methods, site coordinates and their general characteristics are detailed in the electronic supplementary material of Appendix A. Overall, our sites can be described as holm oak woodlands affected by different deforestation intensity levels (but with no signs of agricultural use) on low-gradient terrain (3.8° ± 1.5° hillslope angle). Soils are *Mollic Haploxeralfs* (Soil Survey Staff 1987) over calcare-

Remote-Sensing Estimations of Precipitation-Use Efficiency

The enhanced vegetation index (EVI) is a remote-sensing index that minimizes the influence of soil background and atmospheric conditions for spatial analysis of vegetation dynamics (Huete and others 2002). EVI is strongly sensitive to changes in vegetation canopy and leaf phenology and, therefore, provides a good indicator of the spatiotemporal variations in leaf area and landscape primary production (Pasquato and others 2015). Ponce-Campos and others (2013) showed that the annual integral of EVI (iEVI) is a good remote-sensing estimator ($R^2 = 0.82$) for the annual net primary production (ANPP) across a variety of arid, semi-arid and mesic grasslands and woodlands in Australia and the USA. Previous remote-sensing analysis of *Q. ilex* forests in Spain found that iEVI strongly correlates (Pearson's $R = 0.91$) with tree annual diametric increment and provides an excellent proxy for ANPP in Iberian holm oak woodlands (Garbulsky and others 2013). Therefore, we applied iEVI as an ANPP proxy for the estimation of PUE in our study sites.

We compiled decade-scale (2000–2014) series of EVI for the study sites with a 16-day compositing period from the MODIS Terra satellite (MOD13Q1 product, collection 5) by using the NASA's Earth Observing System Reverb tool (http://reverb.echo.nasa.gov/). The data were re-projected to UTM WGS84 (231×231 m pixel size after re-projection). We checked the reliability summary layer of the MODIS products and discarded those EVI values that were affected by snow, ice and cloud anomalies (1% of data). Discarded values were then interpolated using a second-order polynomial. Finally, the EVI time series were filtered by applying a Savitzky–Golay smoothing algorithm to reduce inherent noise (Choler and others 2010; Moreno-de las Heras and others 2015). iEVI was calculated as the sum of the filtered EVI data for each hydrological year (from present September to August of the following year). PUE was estimated for each site and hydrological year as the ratio of iEVI (dimensionless) to annual precipitation (mm), using the rainfall records of the closest reference weather station. We applied rainfall records of 9 meteorological stations facilitated by the Spanish Agency of Meteorology, AEMET (Figure 1, station ID and coordinates in the electronic supplementary material of Appendix A: Table A2). Site mean dis-tance to the nearest weather station is 6.9 ± 2.9 km. PUE was expressed in 10^{-2} mm^{-1} for analysis to reduce the number of decimal places in the estimation of model coefficients and graphical presentation.

Estimation of Disturbance Intensity Using Local Vegetation Conditions

Tree cover (TC, %) was determined using high-resolution (50 cm per pixel) digital orthophotos of the Spanish National Program for Aerial Orthophotography (PNOA, 2012 campaign). The PNOA orthophotos were downloaded using the IBERPIX web platform (http://www.ign.es/iberpix2/visor/) of the Spanish National Institute of Geography (IGN) and clipped to match the 231×231 m size of the study plots. We used the spectral information of the orthophotos (that is, the red, green and blue bands) to generate binary maps of tree vegetation by applying supervised classification techniques, achieving a mean global accuracy of $95 \pm 4\%$ for the determination of tree cover. Comparison of our remote-sensed estimations of tree vegetation cover with alternative determinations using older (years 2004 or 2006) PNOA orthophotos revealed negligible temporal variations in tree cover ($< 5\%$ in all sites) between 2004/06 and 2012. Consequently, the quantified fractional cover values are representative of the site vegetation conditions for the full (2000–2014) study period.

Vegetation cover patterns in Mediterranean landscapes depend on a variety of factors, including the effects of human disturbance, topographical control of incoming solar radiation, and soil formation and natural erosion processes (Kutiel and Lavee 1998; Grove and Rackham 2001; Bochet and others 2009; Marston 2010). Detailed analysis on the influence of site distance to the nearest settlement (as a proxy of local deforestation by human activities typically concentrated in the proximity of the villages) and landscape geomorphology (that is, hillslope gradient and aspect) on tree cover patterns for our 138 holm oak sites (electronic supplementary material of Appendix B) indicated that tree cover variations within each rural town/hamlet vicinity of the explored region reflect local intensity levels of human disturbance (that is, tree vegetation cover increased with site distance to the nearest human settlement), also discarding any significant topographical effects for these low-gradient terrain landscapes. However, the length of the disturbance (or tree cover reduction) gradients is different for the three climate aridity levels, as

indicated by existing regional differences in maximum tree cover for the climate types. In fact, remote-sensing analysis of tree cover over the complete regional extent of low-gradient ($< 10°$), calcareous holm oak woodlands (920 MODIS pixels, 4900 ha) resulted in maximum values of 87, 75 and 53% cover for sub-humid, dry-transition and semi-arid climate conditions, respectively, suggesting increasing climate limitation for tree cover development along the study aridity gradient. A local deforestation level, Dl, was calculated for each site (as a function of their climate potential for tree cover development) and further applied as a standardized descriptor of disturbance intensity across our aridity gradient:

$$Dl = (TC_{max} - TC)/TC_{max} \quad (1)$$

where TC (%) represents tree cover for a particular site, TC_{max} (%) represents the maximum tree cover level for the corresponding climate type of the analyzed site (given by the above-detailed values for sub-humid, dry-transition and semi-arid conditions), and the local deforestation level (Dl) takes values between 0 for undisturbed (TC = TC_{max}) and 1 for entirely deforested (TC = 0% tree cover) site conditions.

Data Analysis

Precipitation-use efficiency of our 138 holm oak sites was modeled as a quadratic function of disturbance intensity (quantified using the local deforestation level), allowing for separate functions for each climate aridity type (semi-arid, dry-transition and sub-humid). We averaged the PUE values over the 14 hydrological years to model the mean trend, yielding a single value for each of the 138 sites. We fitted the following model:

$$
\begin{aligned}
E(PUE) = &\beta_0 + \beta_1 I_{SA} + \beta_2 I_{DT} + \beta_3 Dl + \beta_4 Dl^2 \\
&+ \beta_5 I_{SA} Dl + \beta_6 I_{DT} Dl + \beta_7 I_{SA} Dl^2 \quad (2) \\
&+ \beta_8 I_{DT} Dl^2
\end{aligned}
$$

where $E(PUE)$ is the mean precipitation-use efficiency (10^{-2} mm^{-1}); I_{SA} is a dummy indicator variable for the semi-arid climate type ($I_{SA} = 1$ if the site is under semi-arid climate and 0 otherwise); I_{DT} is an indicator variable of the dry-transition climate type; Dl is the local deforestation level of the sites; and β_0 through β_8 are parameters to be estimated.

For each climate aridity level, the separate PUE–Dl functions took the form of a second-order polynomial where the intercept, linear, quadratic coefficients and their standard errors were quanti-

fied as linear combinations of the β parameters of equation (2) (electronic supplementary material of Appendix C: equations C2–C4).

We extended the above-described general model to account for the influence of the type of hydrological year (dry *versus* wet years throughout the study period) on the relationship between PUE and disturbance intensity. Dry (wet) years were defined for analysis by using the rainfall records of the reference meteorological stations as those years with precipitation below (above) historical (1998–2014) mean precipitation. We took within-site dry and wet year average PUE values for model computation and extended equation (2) by incorporating a dummy indicator variable for type of year (with values of 1 and 0 for dry and wet year, respectively) as well as all its interactions with climate aridity type and the linear and quadratic terms of the function, totaling 9 additional parameters (electronic supplementary material of Appendix C: equation C5). The model included a random effect for site to account for the lack of independence between dry and wet observations from the same site. We applied a weighed model structure, with weights proportional to the reciprocal of the error variance, to account for differences in the number of observations for dry/wet years among sites. As for the above-described general model, each climate aridity and hydrological year type combination in the extended model was expressed in a separate PUE–Dl function of second-order polynomial structure, where the coefficients and their errors were estimated as linear combinations of the parameters of the extended model (electronic supplementary material of Appendix C: equations C6–C11).

Goodness of fit for the general PUE–Dl model was assessed using the coefficient of determination (R^2). For the extended PUE–Dl model, marginal R^2 (proportion of variance explained by the fixed predictors: local deforestation level, climate aridity level and type of hydrological year) and conditional R^2 (variance explained by both the fixed predictors and the random, site, variable) were calculated following the mathematical approach described by Nakagawa and Schielzeth (2013) for mixed-effect models. Variations in the relationships between PUE and disturbance intensity for the different levels (semi-arid, dry-transition and sub-humid) of climate aridity and (dry/wet) type of hydrological year were assessed by evaluating the size (that is, the absolute values) and statistical significance of the coefficients for the separate PUE–Dl functions.
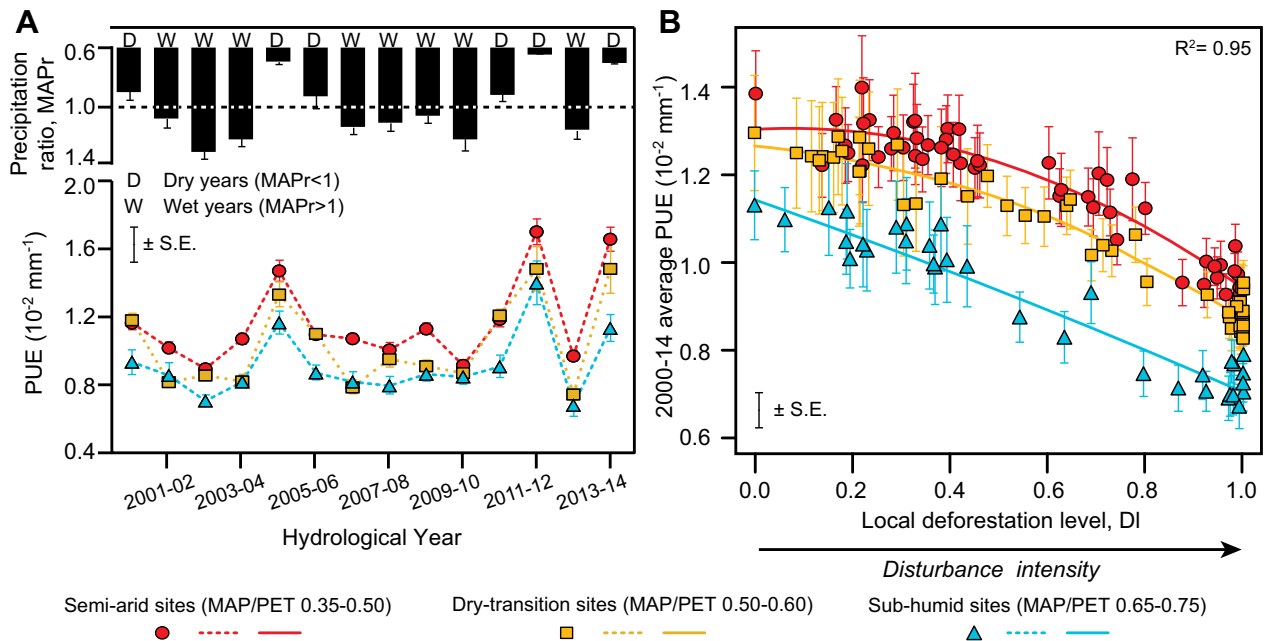
Figure 2. General effects of (**A**) climate conditions (that is, aridity level) and (**B**) disturbance intensity (as described by the local deforestation level, Dl, of the study sites) on precipitation-use efficiency (PUE). Between-year variations of site-averaged PUE values are represented for each climate condition in panel (**A**). 2000–2014 average PUE values for each site and climate condition are detailed in panel (**B**). MAPr in panel (**A**) represents the ratio of present-year precipitation to historical (1998–2014) average precipitation. Reported R^2 and fitted lines in panel (**B**) correspond to the general (14-year average response) model.

RESULTS

PUE for our 138 study holm oak sites varied considerably both between climate aridity levels and among hydrological years (Figure 2A). Vegetation PUE decreased from semi-arid to sub-humid conditions and strongly peaked for the three driest years of the series (hydrological years 2004–2005, 2011–2012 and 2013–2014, with annual precipitation about 60–70% of the historical average precipitation).

Precipitation-use efficiency decreased with increasing local deforestation levels (Dl), overall accounting for an estimated absolute reduction of about 0.4 10^{-2} mm^{-1} (30–35%) of 2000–2014 average PUE, irrespective of climate aridity conditions (Figure 2B). However, the shape of the PUE-reduction trend changed along the aridity gradient, as indicated by the differences in size ($F_{2, 128} = 3.1$; $P = 0.048$) of the separate quadratic terms in the general PUE–Dl model for semi-arid (SA), dry-transition (DT) and sub-humid (SH) climate conditions (Table 1). The curvature (or abruptness) of the relationship between vegetation PUE and disturbance intensity, measured by the absolute values of the quadratic terms in the general PUE–Dl model, increased from SH (− 0.10) to DT (− 0.29)

and SA (− 0.42) sites. Furthermore, lack of significance of the quadratic term in the general PUE–Dl model for SH holm oak sites ($t_{129} = − 0.98$; $P = 0.33$) indicated that 2000–2014 average PUE values decreased linearly with disturbance intensity under sub-humid conditions (Figure 2B). Differently, for dry-transition and semi-arid holm oak sites there was strong evidence that PUE decreased nonlinearly with increased disturbance intensity (DT and SA quadratic terms in the general PUE–Dl model were significant at $P < 0.001$; Table 1).

Our holm oak sites showed higher vegetation PUE for dry than for wet years (Figure 3). The relationship between PUE and disturbance intensity for separate dry and wet years were consistent with the general patterns described for the SA, DT and SH climate aridity levels by the 2000–2014 average PUE–Dl trends. Indeed, the quadratic coefficients of the extended dry/wet model for both DT and SA sites were statistically significant at $P < 0.05$ (Table 1), pointing out accelerated, nonlinear reductions in vegetation PUE with disturbance intensity under semi-arid and dry-transition conditions (Figure 3A, B). Conversely, the quadratic terms of the extended PUE–Dl functions for SH sites were not statistically different from zero for both dry ($t_{129} = − 1.29$; $P = 0.20$) and wet years

Table 1. Equation Fitting Parameter Estimates and Statistics of the Relationship Between PUE and Disturbance Intensity (as Described by the Local Deforestation Level, Dl, of the Study Sites) for the General (14-Year Average Response) and Extended (Dry/Wet Year) Models.

	Intercept	Linear coefficient	Quadratic coefficient
General model: average PUE–Dl relationship			
SA sites			
Estimate	1.30***	0.06^{ns}	− 0.42***
SE	0.02	0.10	0.08
DT sites			
Estimate	1.27***	− 0.11^{ns}	− 0.29***
SE	0.02	0.09	0.08
SH sites			
Estimate	1.14***	− 0.34**	− 0.10^{ns}
SE	0.03	0.11	0.10
Extended model: dry year PUE–Dl relationship			
SA sites			
Estimate	1.64***	− 0.09^{ns}	− 0.47***
SE	0.03	0.13	0.11
DT sites			
Estimate	1.68***	− 0.42***	− 0.20*
SE	0.03	0.12	0.10
SH sites			
Estimate	1.39***	− 0.37*	− 0.17^{ns}
SE	0.04	0.16	0.13
Extended model: wet year PUE–Dl relationship			
SA sites			
Estimate	1.12***	− 0.01^{ns}	− 0.28**
SE	0.03	0.11	0.09
DT sites			
Estimate	0.96***	0.13^{ns}	− 0.35***
SE	0.02	0.10	0.09
SH sites			
Estimate	0.99***	− 0.39**	0.03^{ns}
SE	0.03	0.12	0.10

SA, semi-arid; DT, dry-transition; SH, sub-humid; SE, standard error.
Significance codes: ***P < 0.001; **P < 0.01; *P < 0.05; ^{ns}non significant at P = 0.05.

($t_{129} = 0.31$; $P = 0.76$), evidencing more gradual, linear effects of disturbance on sub-humid holm oak PUE levels (Figure 3C).

Type of hydrological year, as assessed by the statistical differences in dry/wet year coefficients of the extended PUE–Dl model, significantly affected ($F_{2, 137} = 4.3$; $P = 0.015$) the effect of disturbance on PUE levels. In fact, total reduction in PUE across the analyzed disturbance intensity gradients was in general deeper for dry than for wet years (35–40% and 25–35%, respectively; Figure 3). These effects were, however, influenced by the climate aridity conditions of the studied holm oak sites. Global PUE reductions associated with the loss of tree cover under semi-arid and dry-transition conditions were about 1.5 times stronger for dry than for wet years (Figure 3A, B). In contrast, the drop in PUE along the analyzed (Dl) disturbance intensity gradient under sub-humid conditions was equivalent for both dry and wet years, accounting for a homogeneous ~35% reduction in PUE levels (Figure 3C).

DISCUSSION

Precipitation-use efficiency provides an integral measure for exploring the response of vegetation primary production to spatiotemporal changes in precipitation and land uses (Le Houerou 1984; Verón and Paruelo 2010; Gaitán and others 2014). Large-scale analysis of remote-sensed precipitation-use efficiency of vegetation in this study facilitated exploration of the interactions between climate aridity, human disturbance and precipitation variability for the emergence of nonlinear changes in the functionality of Iberian holm oak woodlands.
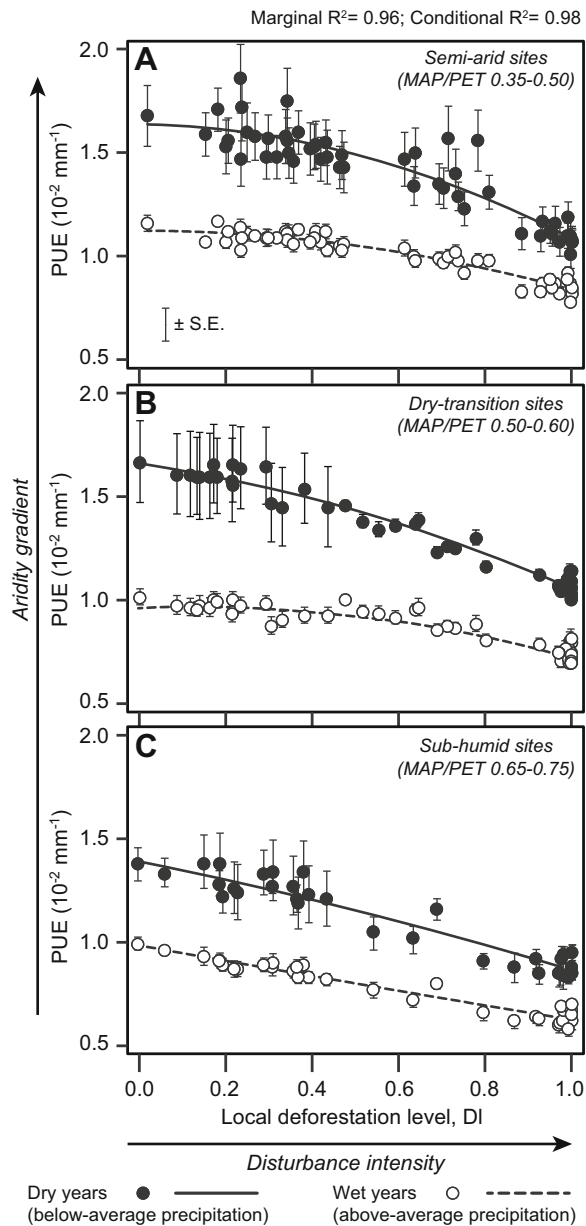
Figure 3. Effect of type of hydrological year (dry versus wet years) on the relationship between precipitation-use efficiency (PUE) and disturbance intensity (as described by the local deforestation levels, Dl, of the study sites) for (**A**) semi-arid, (**B**) dry-transition and (**C**) sub-humid sites. Reported marginal and conditional R^2 (on top of the graph) and fitted lines correspond to the extended (dry/wet year response) model.

PUE decreased from semi-arid to dry-transition and sub-humid conditions in our holm oak sites (Figure 2A), which agrees with other studies that pointed out that as water stress decreases from semi-arid to humid conditions with increasing annual average precipitation, primary production is gradually more constrained by other factors, such as the availability of nutrients and light (Huxman and others 2004; Prince and others 2007; Ruppert and others 2012; Gaitán and others 2014). More importantly, PUE in our study sites also decreased with the intensity of human disturbance (Figure 2B). Accordingly, the precipitation-use efficiency of vegetation has been reported to show a high sensitivity to the alteration of both vegetation and soil conditions (Le Houerou 1984; O'Connor and others 2001; Prince and others 2007). PUE in highly disturbed landscapes generally falls due to enhanced water loss by surface runoff and direct evaporation that, in turn, reduces the proportion of precipitation that is used for transpiration (Ludwig and others 1999; Verón and Paruelo 2010). Our results indicate that the conversion rate of precipitation into vegetation primary production can decrease up to 35% in disturbed Iberian holm oak woodlands. This reduction in PUE values is similar to reported changes for other degraded dryland ecosystems in Australia, Africa and America (Le Houerou 1984; Holm and others 2003; Verón and Paruelo 2010; Moreno-de las Heras and others 2012).

Our findings indicate different precipitation-use efficiency responses to human disturbance of holm oak woodlands as a function of their climate aridity conditions (Figure 2B). Sub-humid conditions showed linear decreases in PUE with increased woodland deforestation. In contrast, semi-arid and dry-transition holm oak sites showed nonlinear decreases in PUE with disturbance intensity; reductions in PUE rapidly accelerated as a quadratic function of local deforestation level. These results provide empirical evidence for the dryland ecosystem stability principles discussed in a variety of theoretical studies, which predict nonlinear behavior for arid and semi-arid ecosystems in response to climate variability and human disturbance (Noy-Meir 1975; Ludwig and others 1999; Scheffer and others 2001; Rietkerk and others 2004; Bestelmeyer and others 2011; Mayor and others 2013). Plant–plant positive interactions (for example, plant facilitation by amelioration of environmental stress), which can effectively provide ecosystem stability to external stressors over a range of vegetation conditions, have been commonly argued to play an important role in the nonlinear behavior of dryland ecosystems (Noy-Meir 1975; Kéfi and others 2007, 2016; Soliveres and others 2015). Similarly, short-range spatial redistribution of water, nutrients, sediments and propagules between bare and vegetated areas is postulated as a fundamental feedback process for structuring and providing stability to dryland

ecosystems with patchy vegetation (Saco and Moreno-de las Heras 2013; Okin and others 2015; Bochet 2015). Both plant–plant interactions and short-range spatial redistribution of surface resources may play a role in the nonlinear behavior of the studied Mediterranean-dry woodlands, where vegetation cover is patchy (that is, tree vegetation for our study sites reached 50–70% maximum cover under semi-arid and dry-transition conditions) and holm oak trees have a key importance in regulating plant–plant interactions and plant–soil feedbacks (Terradas 1999; Cubera and Moreno 2007; Carnicer and others 2013). Significant deterioration of these stabilizing feedbacks (for example, loss of large vegetation patches with high capacity to modify environmental conditions) may induce accelerated, rapid loss of ecosystem function (Kéfi and others 2007; Moreno-de las Heras and others 2012; Berdugo and others 2017).

Precipitation-use efficiency of vegetation was considerably higher for dry than for wet years across 2000–2014 in our study holm oak sites (Figures 2A and 3), which agrees with other studies that perceived similar variations in PUE as an ecosystem resilience mechanism that sustains vegetation production during the driest periods (Huxman 2004; Wessels and others 2007; Ponce-Campos and others 2013; Zhang and others 2014). In general, disturbance induced a stronger decline in PUE values for dry than for wet years resulting, for severely altered landscapes, in a sharp reduction in the ecosystem ability to buffer large changes on primary production caused by drought (Figure 3). In fact, the alteration of landscape conditions in dryland ecosystems typically shows more pronounced effects on primary production and precipitation-use efficiency of vegetation during dry periods, which strongly affects the vulnerability of disturbed landscapes to precipitation variability (Pickup 1996; Dube and Pickup 2001; Hein 2006). For example, the scarcity of deep-rooted trees under the most disturbed conditions of our holm oak study sites very likely constrains vegetation use of deep soil moisture, which has been argued to play an important role in retaining primary production during dry periods in Mediterranean oak woodlands (Baldocchi and Xu 2007; Cubera and Moreno 2007).

The differences between dry and wet years on the response of PUE to disturbance increased with aridity from sub-humid conditions (where PUE reductions with site deforestation were equivalent for both dry and wet years, Figure 3C) to dry-transition and semi-arid conditions (1.5 times stronger PUE drop along the disturbance gradient for dry than for wet years, Figure 3A, B), suggesting that aridity in the studied Iberian holm oak woodlands may intensify the vulnerability of ecosystems to the combined effects of climate variability and disturbance. The previous analysis of arid to mesic Mediterranean rangelands affected by grazing pointed to a similar reduction in resilience to climate-driven changes in vegetation production that is exacerbated by climate aridity, which may facilitate the collapse of ecosystem functions and services by drought in intensively used dry landscapes (Köchy and others 2008).

In sum, our results indicate that the interaction of climate variability and human disturbance in Iberian holm oak woodlands can result in nonlinear decreases in ecosystem function under semi-arid and dry-transition climate conditions. Changes in climate aridity and drought frequency are currently perceived as chronic contributors to ecosystem degradation in drylands (Suding and others 2004; Moreno-de las Heras and others 2012). Climate change projections for the Iberian Peninsula suggest decreased mean annual rainfall with increased summer temperatures and drought frequency for the next 100 years (de Castro and others 2005), which may exacerbate ecosystem change in Iberian holm oak woodlands. Specifically, sub-humid holm oak woodlands, showing at present gradual, linear reductions in ecosystem function in response to the effects of human disturbance, may also acquire the characteristic nonlinear behavior of the semi-arid and dry-transition sites. There is particular concern that, under certain circumstances, these nonlinear ecosystem changes can be largely irreversible (Noy-Meir 1975; Schlesinger and others 1990; Scheffer and others 2001; Rietkerk and others 2004; Kéfi and others 2016). Historical environmental records indicate that deforestation of Iberian holm oak woodlands at the boundary between arid and semi-arid climate conditions (MAP-to-PET ratio 0.20–0.40) can result in persistent ecosystem changes (Latorre and others 2001). Biodiversity and soil conditions (for example, water retention capacity, soil biological activity, nutrient cycling integrity) play a fundamental role in conferring stability and resilience to dryland ecosystems (Suding and others 2004; García-Fayos and Bochet 2009; Maestre and others 2016). Further exploration of biodiversity patterns and soil functions may assist ascertaining whether observed nonlinear reductions in PUE levels of Iberian holm oak woodlands may hinder natural recovery of disturbed ecosystems.

REFERENCES

Bai Z, Dent D, Wu Y, de Jong R. 2013. Land degradation and ecosystem services. In: Lal R, Lorenz K, Hüttl RF, Schneider BU, von Braun J, Eds. Ecosystem services and carbon sequestration in the biosphere. Dordrecht: Springer. p 357–81.

Baldocchi DD, Xu L. 2007. What limits evaporation from Mediterranean oak woodlands—The supply of moisture in the soil, physiological control by plants or the demand by the atmosphere? Adv Water Resour 30:2113–22.

Berdugo M, Kéfi S, Soliveres S, Maestre FT. 2017. Plant spatial patterns identify alternative ecosystem multifunctionality states in global drylands. Nat Ecol Evol 9:0003. https://doi.org/10.1038/s41559-016-0003.

Bestelmeyer B, Ellison AM, Fraser WR, Gorman KB, Holbrook SJ, Laney CM, Ohman MD, Peters DPC, Pillsbury FC, Rassweiler A, Schmitt RJ, Sharma S. 2011. Analysis of abrupt transitions in ecological systems. Ecosphere 2:1–26.

Bochet E. 2015. The fate of seeds in the soil: a review of the influence of overland flow on seed removal and its consequences for the vegetation of arid and semiarid patchy ecosystems. Soil 1:131–46.

Bochet E, Garcia-Fayos P, Poesen J. 2009. Topographic thresholds for plant colonization on semi-arid eroded slopes. Earth Surf Proc Land 34:1758–71.

Carnicer J, Barbeta A, Sperlich D, Coll M, Peñuelas J. 2013. Contrasting trait syndromes in angiosperms and conifers are associated with different responses of tree growth to temperature on a large scale. Front Plant Sci 4:1–19.

Choler P, Sea W, Briggs P, Rapauch M, Leuning R. 2010. A simple ecohydrological model captures essentials of seasonal leaf dynamics in semi-arid tropical grasslands. Biogeosciences 7:907–20.

Cubera E, Moreno G. 2007. Effect of single *Quercus ilex* trees upon spatial and seasonal changes in soil water content in dehesas of central western Spain. Ann For Sci 64:355–64.

de Castro M, Martín-Vide J, Alonso S. 2005. The climate of Spain: past, present and scenarios for the 21th century. In: Moreno-Rodriguez JM, Ed. A preliminary general assessment in Spain due to the effects of climate change. Madrid: Ministerio de Medio Ambiente. p 1–62.

Dube OP, Pickup G. 2001. Effects of rainfall variability and communal and semi-commercial grazing on land cover in southern African rangelands. Clim Res 17:195–208.

Gaitán JJ, Oliva GE, Bran DE, Maestre FT, Aguiar MR, Jobbágy EG, Buono GG, Ferrante D, Nakamatsu VB, Ciari G, Salomone JM, Massara V. 2014. Vegetation structure is important for explaining ecosystem function across Patagonian rangelands. J Ecol 102:1419–28.

Garbulsky M, Peñuelas J, Ogaya R, Filella I. 2013. Leaf and stand-level carbon uptake of a Mediterranean forest estimated using the satellite-derived reflectance indices EVI and PRI. Int J Remote Sens 34:1282–96.

García-Fayos P, Bochet E. 2009. Indication of antagonistic interaction between climate change and erosion on plant species richness and soil properties in semiarid Mediterranean ecosystems. Glob Change Biol 15:306–18.

Grove AT, Rackham O. 2001. The nature of Mediterranean Europe: an ecological history. New Haven: Yale University Press.

Hein L. 2006. The impacts of grazing and rainfall variability on the dynamics of the Sahelian rangeland. J Arid Environ 64:488–504.

Holm AMcR, Watson IW, Loneragan WA, Adams MA. 2003. Loss of patch-scale heterogeneity on primary productivity and rainfall-use efficiency in Western Australia. Basic Appl Ecol 4:569–78.

Huete A, Didan K, Miura T, Rodriguez EP, Gao X, Ferreira LG. 2002. Overview of the radiometric and biophysical performance of the MODIS vegetation indices. Remote Sens Environ 83:195–213.

Huxman TE, Smith MD, Fay PA, Knapp AK, Shaw MR, Loik ME, Smith SD, Tissue DT, Zak JC, Weltzin JF, Pockman WT, Sala OE, Haddad BM, Harte J, Koch GW, Schwinning S, Small EE, Williams DG. 2004. Convergence across biomes to a common rain-use efficiency. Nature 429:651–4.

Kéfi S, Rietkerk M, Alados CL, Pueyo Y, Papanastasis VP, ElAich A, de Ruiter PC. 2007. Spatial vegetation patterns and imminent desertification in Mediterranean arid ecosystems. Nature 449:213–18.

Kéfi S, Holmgren M, Scheffer M. 2016. When can positive interactions cause alternative stable states in ecosystems? Funct Ecol 30:88–97.

Köchy M, Mathaj M, Jeltsch F, Malkinson D. 2008. Resilience of stocking capacity to changing in arid to Mediterranean landscapes. Reg Environ Change 8:73–87.

Kutiel P, Lavee H. 1998. Effect of slope aspect on soil and vegetation properties along an aridity transect. Isr J Plant Sci 47:169–78.

Latorre JG, García-Latorre J, Sánchez-Picón A. 2001. Dealing with aridity: socio-economic structures and environmental changes in an arid Mediterranean region. Land Use Pol 18:53–64.

Le Houerou HN. 1984. Rain use efficiency: a unifying concept in arid-land ecology. J Arid Environ 7:213–47.

Ludwig JA, Tongway DJ, Mardsen SG. 1999. Stripes, strands or stipples: modelling the influence of three landscape banding patterns on resource capture and productivity in semi-arid woodlands, Australia. Catena 37:257–73.

Maestre FT, Eldridge DJ, Soliveres S, Kéfi S, Delgado-Baquerizo M, Bowker MA, García-Palacios P, Gaitán J, Gallardo A, Lázaro R, Berdugo M. 2016. Structure and functioning of dry-

land ecosystems in a changing world. Annu Rev Ecol Evol Syst 47:215–37.

Marston RA. 2010. Geomorphology and vegetation on hillslopes: interactions, dependencies and feedback loops. Geomorphology 116:206–17.

Martínez-Valderrama J, Ibáñez J, del Barrio G, Sanjuán ME, Alcalá FJ, Martínez-Vicente S, Ruiz A, Puigdefábregas J. 2016. Present and future of desertification in Spain: implementation of a surveillance system to prevent land degradation. Sci Total Environ 563–564:169–78.

Mayor AG, Kéfi S, Bautista S, Rodríguez F, Cartení F, Rietkerk M. 2013. Feedbacks between vegetation pattern and resource loss dramatically decrease ecosystem resilience and restoration potential in a simple dryland model. Landsc Ecol 28:931–42.

McLean IMD, Willson RJ. 2011. Recent ecological responses to climate change support predictions of high extinction risk. Proc Natl Acad Sci USA 108:12337–42.

Millennium Ecosystem Assessment. 2005. Ecosystems and human wellbeing: biodiversity synthesis. Washington, DC: World Resources Institute.

Moreno-de las Heras M, Saco PM, Willgoose GR, Tongway DJ. 2012. Variations of hydrological connectivity of Australian semiarid landscapes indicate abrupt changes in rainfall-use efficiency of vegetation. J Geophys Res Biogeosci 117:G03009. https://doi.org/10.1029/2011jg001839.

Moreno-de las Heras M, Díaz-Sierra R, Turnbull L, Wainwright J. 2015. Assessing vegetation structure and ANPP dynamics in a grassland-shrubland Chihuahuan ecotone using NDVI-rainfall relationships. Biogeosciences 12:2907–25.

Nakagawa S, Schielzeth H. 2013. A general and simple method for obtaining R^2 from generalized linear mixed-effect models. Methods Ecol Evol 4:133–42.

Noy-Meir I. 1975. Stability of grazing systems: an application of predator-prey graphs. J Ecol 63:459–81.

O'Connor TG, Haines LM, Snyman HA. 2001. Influence of precipitation and species composition on phytomass of a semi-arid African grassland. J Ecol 89:850–60.

Okin GS, Moreno-de las Heras M, Saco PM, Throop HL, Vivoni ER, Parsons AJ, Wainwright J, Peters DPC. 2015. Connectivity in dryland landscapes: shifting concepts of spatial interactions. Front Ecol Environ 13:20–7.

Pasquato M, Medici C, Friend AD, Francés F. 2015. Comparing two approaches for parsimonious vegetation modelling in semiarid regions using satellite data. Ecohydrology 8:1024–36.

Peters DPC, Bestelmeyer BT, Herrick JE, Fredrickson EL, Monger HC, Havstad KM. 2006. Disentangling complex landscapes: new insights to forecasting arid and semi-arid system dynamics. BioScience 56:491–501.

Pickup G. 1996. Estimating the effects of land degradation and rainfall variation on productivity in rangelands: an approach using remote sensing and models of grazing and herbage dynamics. J Appl Ecol 33:819–32.

Ponce-Campos GE, Moran AS, Huete A, Zhand Y, Bresloff C, Huxman TE, Eamus D, Bosch DD, Buda AR, Gunter SA, Scalley TH, Kitchen SG, McClaran MP, McNab WH, Montoya DS, Morgan JA, Peters DPC, Sadler EJ, Seyfred MS, Starks PJ. 2013. Ecosystem resilience despite large-scale altered hydroclimatic conditions. Nature 494:349–53.

Prince SD, Wessels KJ, Tucker CJ, Nicholson SE. 2007. Desertification in the Sahel: a reinterpretation of a reinterpretation. Glob Change Biol 13:1308–13.

Rietkerk M, Dekker SC, de Ruiter PC, van de Koppel J. 2004. Self-organized patchiness and catastrophic shifts in ecosystems. Science 305:1926–9.

Ruppert JC, Holm A, Miehe S, Muldavin E, Snyman HA, Wesche K, Linstädter A. 2012. Meta-analysis of ANPP and rain-use efficiency confirms indicative value for degradation and supports non-linear response along precipitation gradients in drylands. J Veg Sci 23:1035–50.

Saco PM, Moreno-de las Heras M. 2013. Ecogeomorphic coevolution of semiarid hillslopes: Emergence of banded and striped vegetation patterns through interaction of biotic and abiotic processes. Water Resour Res 49:115–26.

Scheffer M, Carpenter S, Foley JA, Folke C, Walker B. 2001. Catastrophic shifts in ecosystems. Nature 413:591–6.

Schlesinger WH, Reynolds JF, Cunningham GL, Huenneke LF, Jarrell WM, Virginia RA, Whithford WG. 1990. Biological feedbacks in global desertification. Science 247:1043–8.

Soil Survey Staff. 1987. Keys to soil taxonomy. Ithaca: US Department of Agriculture, Soil Management Support Services, Cornell University.

Soliveres S, Smith C, Maestre FT. 2015. Moving forward on facilitation research: response to changing environments and effects on the diversity, functioning and evolution of plant communities. Biol Rev 90:297–313.

Stevenson AC. 2000. The Holocene forest history of the Montes Universales, Teruel, Spain. The Holocene 10:603–10.

Suding KN, Gross KL, Houseman GR. 2004. Alternative states and positive feedbacks in restoration ecology. Trends Ecol Evol 19:46–53.

Terradas J. 1999. Holm oak and holm oak forests: an introduction. In: Rodà F, Retana J, Gracia CA, Bellot J, Terradas J, Eds. Ecology of Mediterranean evergreen forests. Berlin: Springer. p 3–14.

UNEP. 1992. World atlas of desertification. United Nations Environmental Program (UNEP). London: Edward Arnold.

Valiente-Baunet A, Verdú M. 2013. Human impacts on multiple ecological networks act synergistically to drive ecosystem collapse. Front Ecol Environ 11:408–13.

Verón SR, Paruelo JM. 2010. Desertification alters the response of vegetation to changes in precipitation. J Appl Ecol 47:1233–41.

Wessels KJ, Prince SD, Malherbe J, Small J, Frost PE, VanZyl D. 2007. Can human-induced land degradation be distinguished from the effects of rainfall variability? A case of study in South Africa. J Arid Environ 68:271–97.

Xu C, Van Nes EH, Holmgran M, Kéfi S, Scheffer M. 2015. Local facilitation may cause tipping points on a landscape level preceded by early warning indicators. Am Nat 186:81–90.

Zhang X, Moran MS, Zhao X, Liu S, Zhou T, Ponce-Campos GE, Liu F. 2014. Impact of prolonged drought on rainfall use efficiency using MODIS data across China in the early 21st century. Remote Sens Environ 150:188–97.

Appendix A: This appendix contains details for the site selection methods

Our site selection procedure aimed to identify a large number of holm oak woodland sites along a climate aridity gradient (semi-arid, dry-transition, and sub-humid conditions with MAP/PET 0.35-0.50, 0.50-0.60, and 0.65-0.75, respectively) affected by different levels of deforestation, with nearby availability of reference meteorological records of precipitation, and minimizing, at the same time, between-site variations on landscape topography and lithology. Site selection was carried out by using (a) large-scale spatial exploration using GIS techniques with thematic information (i.e. climate, land cover type, elevation, slope gradient, and lithology), and (b) further field validation within an approx. 20,000 km^2 region in eastern Spain (Figure 1 in the paper).

As sources for the GIS thematic information for the site selection, we used:

- Climate data: the Digital Climate Atlas of the Iberian Peninsula (Ninyerola and others 2005) and the Global Potential Evapo-Transpiration dataset developed by the Consortium of International Agricultural Research Centers (Trabucco and Zomer 2009) with 200 and 1000 m resolution, respectively.
- Land cover type data: the European CLC2006 land use map (100 m resolution) developed by the Corine Land Cover EU Program (EEA 2007).
- Elevation and slope gradient: the Digital Elevation Model MDT25 (25 m resolution, mean square error 50 cm) developed with LiDAR technologies within the Spanish National Plan for Earth Observation (PNOA) and distributed by the Spanish National Geographic Institute (IGN).
- Lithology: the 1:50,000 National Geological Map of Spain (IGME 2012).

We applied a GIS raster mesh with pixel size 231 x 231 m (UTM WGS84 projection) derived from the MOD13Q1 product of the Moderate Resolution Spatial Spectroradiometer (MODIS) to initiate the site selection. First, we determined within the 20,000 km^2 region those potential areas with (i) natural forests and open woodlands (excluding sites dominated by coniferous vegetation), (ii) elevation <1500 m.a.s.l. (the regional orographic limit for the distribution of holm oak; Longares-Aladren and Mateo-Sanz 2014), (iii) slope gradient <10°, (iv) calcareous lithology (limestones and dolomites of Cretaceous or Jurassic age), and (v) <15 km distance to the closest weather station of the Spanish Agency of Meteorology (AEMET) with available precipitation data. Further visual analysis of the potential areas using high resolution (50 cm) aerial photographs distributed by the IGN through the IBERPIX platform (http://www.ign.es/iberpix2/visor/) facilitated the selection of a wide range of study sites with different deforestation levels: from the maximum tree cover detected for each climate aridity level (about 55, 75 and 90% for semi-arid, dry-transition and sub-humid climate conditions, respectively) to

approximately 0% tree cover. Site characteristics (e.g. dominance of *Quercus ilex*, vegetation condition, soil type) were subsequently verified in the field. A total of 138 sites (53, 51 and 34 sites for semi-arid, dry-transition and sub-humid conditions, respectively) of 231 x 231 m were selected. In order to increase the independence of the plots, no single plot shared any side with the other plots. Site coordinates and general characteristics are detailed below in Table A1 of this appendix. The AEMET identification codes, coordinates and elevation of the 9 weather stations that were applied in this study are also detailed below in Table A2 of this appendix.

Table A1. Site center coordinates (UTM WGS84, Zone 30 North) and general characteristics (i.e. elevation; slope angle; mean annual precipitation, MAP; potential evapotranspiration, PET; MAP/PET ratio; mean annual temperature, MAT; tree cover, TC; and deforestation level, Dl) for the 138 holm oak study sites. Each site has a size of 231 x 231 m.

Site ID	Easting (m)	Northing (m)	Elevat.[1] (m.a.s.l.)	Slope[1] (°)	MAP[2] (mm)	PET[3] (mm)	MAP/PET	MAT[2] (ºC)	TC[4] (%)	Dl[5]
Semi-arid sites (MAP/PET 0.35-0.50)										
S1	632004	4483237	1268	3.1	440	926	0.48	10.7	30.4	0.43
S2	632004	4482310	1246	2.9	442	924	0.48	10.8	40.4	0.25
S3	632236	4482079	1227	6.1	438	921	0.48	10.8	41.1	0.23
S4	633394	4483237	1257	5.6	425	923	0.46	10.6	52.7	0.02
S5	633857	4483005	1260	3.4	379	924	0.41	10.7	35.6	0.34
S6	634552	4501769	1175	4.3	444	926	0.48	10.7	44.0	0.18
S7	634784	4482079	1267	3.3	432	925	0.47	10.7	43.0	0.20
S8	635016	4501769	1195	5.0	449	926	0.48	10.7	42.7	0.21
S9	635016	4482774	1290	2.7	423	925	0.46	10.6	35.2	0.34
S10	636869	4497600	1147	6.9	449	929	0.48	11.0	39.4	0.27
S11	636869	4495283	1200	6.2	350	929	0.38	10.4	45.5	0.15
S12	637101	4497831	1155	2.1	448	923	0.49	11.0	34.0	0.37
S13	637332	4489955	1162	4.9	425	923	0.46	10.6	31.8	0.41
S14	637332	4479530	1206	3.1	432	915	0.47	10.9	31.3	0.42
S15	637564	4498063	1139	3.1	448	923	0.49	11.0	35.4	0.34
S16	637564	4479994	1209	2.6	433	913	0.47	10.9	38.0	0.29
S17	637796	4489955	1143	5.3	423	919	0.46	10.8	30.6	0.43
S18	638027	4490187	1147	5.6	430	920	0.47	10.7	32.0	0.40
S19	638491	4489260	1133	3.3	432	920	0.47	10.7	28.9	0.46
S20	638722	4489028	1121	4.0	435	919	0.47	10.8	16.6	0.69
S21	638954	4491345	1118	2.4	444	925	0.48	10.7	2.2	0.96
S22	638954	4488565	1112	4.2	450	929	0.48	10.8	19.7	0.63
S23	639186	4492040	1073	6.5	446	920	0.48	10.7	0.1	1.00
S24	639186	4491577	1118	1.4	437	927	0.47	10.7	1.6	0.97
S25	639186	4491113	1119	2.1	424	926	0.46	10.7	13.4	0.75
S26	639186	4486943	1126	6.4	449	926	0.48	10.9	16.0	0.70
S27	639417	4490650	1109	4.3	434	929	0.47	10.7	3.7	0.93
S28	639417	4486712	1115	5.7	429	929	0.46	11.0	10.4	0.81
S29	639881	4491577	1063	6.4	439	927	0.47	10.6	0.0	1.00
S30	639881	4486480	1099	4.5	423	929	0.46	11.0	0.6	0.99
S31	640112	4491113	1067	7.3	430	929	0.46	10.6	0.3	1.00
S32	640344	4501306	984	2.9	442	928	0.48	11.6	0.3	0.99
S33	640344	4489723	1091	5.2	459	927	0.5	10.8	6.3	0.88

Table A1 continuation (1).

Site ID	Easting (m)	Northing (m)	Elevat.[1] (m.a.s.l.)	Slope[1] (º)	MAP[2] (mm)	PET[3] (mm)	MAP/PET	MAT[2] (ºC)	TC[4] (%)	Dl[5]

Site ID	Easting (m)	Northing (m)	Elevat.[1] (m.a.s.l.)	Slope[1] (º)	MAP[2] (mm)	PET[3] (mm)	MAP/PET	MAT[2] (ºC)	TC[4] (%)	Dl[5]
Semi-arid sites (MAP/PET 0.35-0.50)										
S34	640575	4489492	1081	5.0	411	928	0.44	10.8	4.0	0.93
S35	640807	4489260	1065	5.4	414	927	0.45	10.9	2.6	0.95
S36	641039	4483932	1096	6.1	423	929	0.46	11.1	14.2	0.74
S37	641502	4489260	1050	4.6	413	930	0.44	11.0	0.1	1.00
S38	641502	4483469	1074	5.7	413	931	0.44	11.2	2.8	0.95
S39	641734	4483237	1072	6.3	410	929	0.44	11.3	0.6	0.99
S40	651695	4466326	1124	2.9	440	929	0.47	11.7	15.4	0.71
S41	651927	4466094	1116	2.0	441	930	0.47	11.7	11.8	0.78
S42	652158	4466558	1077	5.6	444	932	0.48	11.8	35.4	0.34
S43	652390	4466094	1088	4.9	447	933	0.48	11.7	41.2	0.23
S44	653317	4465399	1070	2.5	431	933	0.46	12.0	41.0	0.24
S45	654012	4483932	1204	5.3	429	935	0.46	10.9	19.5	0.64
S46	633394	4482310	1232	4.6	433	936	0.46	10.8	28.4	0.47
S47	633857	4482310	1235	2.8	428	937	0.46	10.8	14.5	0.73
S48	634089	4482079	1233	5.5	436	938	0.46	10.8	20.9	0.61
S49	635016	4481384	1246	3.5	426	938	0.45	10.8	28.6	0.47
S50	636869	4490187	1191	3.8	443	940	0.47	10.5	34.6	0.36
S51	637101	4492272	1188	6.3	444	940	0.47	10.4	36.7	0.32
S52	637796	4481384	1235	5.1	433	943	0.46	10.8	37.7	0.30
S53	639186	4481152	1210	3.7	423	909	0.47	10.9	32.5	0.39
Dry-transition sites (MAP/PET 0.50-0.60)										
S54	606290	4539066	1168	2.1	508	941	0.54	11.1	0.7	0.99
S55	606522	4538603	1162	1.1	505	939	0.54	11.1	0.2	1.00
S56	606754	4538834	1163	1.1	500	939	0.53	11.1	0.9	0.99
S57	606985	4539298	1176	2.1	501	939	0.53	11.1	39.0	0.48
S58	606985	4538603	1163	1.1	503	941	0.53	11.1	0.2	1.00
S59	607217	4539066	1163	3.3	504	941	0.54	11.1	30.3	0.59
S60	607449	4537908	1157	3.3	515	940	0.55	11.1	0.0	1.00
S61	607680	4538139	1153	3.4	506	939	0.54	11.1	0.5	0.99
S62	607680	4537676	1147	4.3	509	940	0.54	11.1	0.0	1.00
S63	607912	4537908	1150	2.9	503	939	0.54	11.1	0.6	0.99
S64	607912	4537445	1143	3.2	507	942	0.54	11.1	0.1	1.00
S65	608144	4538834	1146	3.6	490	941	0.52	11.1	20.0	0.73
S66	608144	4538139	1133	5.5	505	943	0.54	11.1	1.8	0.98
S67	608144	4537676	1144	3.1	506	942	0.54	11.1	0.4	0.99
S68	608144	4537213	1134	3.9	503	943	0.53	11.1	0.1	1.00
S69	608375	4538603	1138	3.9	507	940	0.54	11.1	21.4	0.71
S70	608375	4537908	1133	2.8	503	942	0.53	11.1	0.4	0.99
S71	608375	4537445	1136	3.9	502	942	0.53	11.1	0.5	0.99
S72	608607	4539298	1140	4.3	497	945	0.53	11.1	26.9	0.64
S73	608607	4536981	1114	5.6	507	941	0.54	11.1	0.0	1.00
S74	609070	4536981	1111	4.2	504	942	0.54	11.1	0.0	1.00
S75	609302	4538603	1128	4.8	497	943	0.53	11.1	14.7	0.80
S76	609765	4538834	1140	3.8	495	940	0.53	11.1	23.1	0.69
S77	612545	4537908	1118	5.7	494	947	0.52	11.1	1.0	0.99
S78	612777	4537676	1114	4.2	494	948	0.52	11.1	2.2	0.97
S79	612777	4536981	1109	2.3	497	943	0.53	11.1	0.0	1.00

Table A1 continuation (2).

Site ID	Easting (m)	Northing (m)	Elevat.[1] (m.a.s.l.)	Slope[1] (°)	MAP[2] (mm)	PET[3] (mm)	MAP/PET	MAT[2] (°C)	TC[4] (%)	DI[5]
S80	613240	4536750	1107	1.5	496	943	0.53	11.1	0.1	1.00
S81	613703	4537213	1099	2.2	492	941	0.52	11.1	0.1	1.00
S82	614630	4536981	1081	2.7	497	940	0.53	11.1	2.2	0.97
S83	615557	4536750	1069	5.2	495	939	0.53	11.1	5.5	0.93
S84	679957	4446404	1182	1.8	517	939	0.55	11.5	58.4	0.22
S85	680189	4446635	1174	2.5	523	939	0.56	11.6	61.7	0.17
S86	680189	4446172	1179	3.2	520	940	0.55	11.5	64.1	0.14
S87	680189	4445709	1190	3.8	491	940	0.52	11.4	51.8	0.30
S88	680420	4446404	1169	2.2	528	922	0.57	11.6	58.4	0.21
S89	680420	4445940	1180	2.8	508	923	0.55	11.5	65.8	0.12
S90	680652	4446635	1159	2.5	495	922	0.54	11.7	74.4	0.00
S91	680652	4445709	1179	2.4	506	920	0.55	11.5	62.4	0.16
S92	680884	4446404	1157	2.3	505	922	0.55	11.7	68.1	0.09
S93	680884	4445940	1164	5.0	500	921	0.54	11.6	57.1	0.23
S94	680884	4445477	1170	2.9	512	924	0.55	11.6	58.5	0.21
S95	681347	4447330	1090	4.3	498	922	0.54	11.8	49.9	0.33
S96	681347	4445940	1166	4.4	495	923	0.54	11.7	46.0	0.38
S97	681579	4445709	1162	4.2	494	923	0.54	11.8	64.6	0.13
S98	681810	4445477	1138	5.6	479	923	0.52	11.8	52.7	0.29
S99	683432	4446404	1043	6.4	504	932	0.54	12.1	42.0	0.44
S100	683664	4446172	1025	4.0	496	925	0.54	12.1	61.1	0.18
S101	607449	4539298	1167	3.1	499	926	0.54	11.1	26.4	0.65
S102	607680	4539066	1159	2.6	513	927	0.55	11.1	16.4	0.78
S103	607912	4539298	1164	2.3	490	938	0.52	11.1	36.0	0.52
S104	608839	4539066	1121	5.8	499	938	0.53	11.1	33.2	0.55
Sub-humid sites (MAP/PET 0.65-0.75)										
S105	597024	4501769	1423	4.8	655	928	0.71	9.7	59.7	0.31
S106	601657	4501769	1431	4.5	623	929	0.67	9.7	66.7	0.23
S107	601889	4502001	1438	2.3	619	881	0.70	9.7	67.3	0.22
S108	602121	4503854	1399	4.8	647	932	0.69	9.8	73.4	0.15
S109	602816	4502928	1424	3.3	606	928	0.65	9.7	59.6	0.31
S110	602816	4502464	1443	2.5	607	926	0.66	9.7	55.6	0.36
S111	603047	4502696	1435	3.0	607	935	0.65	9.7	52.5	0.39
S112	603279	4503854	1377	2.6	614	925	0.66	9.9	48.9	0.43
S113	603510	4504318	1357	2.8	606	924	0.66	10.1	54.6	0.37
S114	604437	4503623	1388	2.8	631	924	0.68	10.0	61.5	0.29
S115	604437	4503159	1394	4.9	643	930	0.69	9.8	70.2	0.19
S116	604669	4503391	1380	4.4	612	933	0.66	10.0	53.6	0.38
S117	729763	4485090	1267	5.4	608	929	0.65	10.9	0.0	1.00
S118	730226	4478835	1269	4.8	652	873	0.75	10.4	81.2	0.06
S119	730458	4477214	1214	4.2	655	870	0.75	10.5	69.6	0.20
S120	730690	4478835	1245	4.3	654	872	0.75	10.5	54.9	0.37
S121	730921	4477214	1194	2.3	640	872	0.73	10.8	31.7	0.63
S122	731153	4478604	1267	4.2	622	876	0.71	10.6	70.3	0.19
S123	731153	4477909	1211	4.8	630	876	0.72	10.7	86.5	0.00
S124	731616	4482310	1125	5.8	645	877	0.74	11.3	39.6	0.54
S125	731616	4477214	1180	2.1	634	888	0.71	10.8	2.6	0.97
S126	731848	4476982	1177	2.3	634	881	0.72	10.8	2.4	0.97

Table A1 continuation (3).

Site ID	Easting (m)	Northing (m)	Elevat.[1] (m.a.s.l.)	Slope[1] (º)	MAP[2] (mm)	PET[3] (mm)	MAP/PET	MAT[2] (ºC)	TC[4] (%)	Dl[5]
S127	731848	4475592	1196	3.3	613	882	0.70	10.9	27.0	0.69
S128	732080	4475129	1177	1.4	633	881	0.72	11.1	11.5	0.87
S129	732311	4477677	1184	3.9	665	883	0.75	11.0	1.8	0.98
S130	732311	4476519	1164	3.8	646	884	0.73	11.0	7.2	0.92
S131	732311	4476056	1167	1.4	638	885	0.72	10.9	0.7	0.99
S132	732543	4481615	1149	4.6	634	884	0.72	10.9	6.6	0.92
S133	732543	4476751	1160	1.5	640	885	0.72	11.0	1.6	0.98
S134	733006	4480920	1142	1.6	627	886	0.71	11.0	2.1	0.98
S135	733933	4476519	1193	4.8	627	885	0.71	10.8	17.7	0.80
S136	736481	4483237	1261	3.1	605	870	0.70	11.0	0.1	1.00
S137	736713	4483469	1258	2.5	638	871	0.73	11.2	0.1	1.00
S138	736945	4483005	1253	2.0	646	871	0.74	11.1	0.0	1.00

Notes: ([1]) Elevation and slope angle values were taken from the PNOT MDT25 digital elevation model (25 m resolution, RMSE 50 cm); ([2]) mean annual precipitation (MAP) and temperature (MAT) values were taken from the Digital Climatic Atlas of the Iberian Peninsula (Ninyerola and others 2005); ([3]) Hargreaves' potential evapotranspiration (PET) values were taken from the CGIAR global-PET dataset (Trabucco and Zomer 2009); ([4]) tree cover (TC) values were determined by applying supervised classification to recent high-resolution (50 cm) digital orthophotos (details in the methods of the paper); ([5]) local deforestation levels (Dl) for the sites were calculated by balancing site tree cover by the maximum tree cover found for each aridity level (53%, 75% and 87% for semi-arid, dry-transition and sub-humid conditions, respectively) following equation 1 (details in the methods of the paper).

Table A2. Station coordinates (UTM WGS84, Zone 30 North), elevation and identification for the 9 AEMET weather stations used to obtain the rainfall records for this study.

Station ID	Easting (m)	Northing (m)	Elevation (m.a.s.l.)	Name of town/location
8355	629414	4491331	1410	Pozondón
8356U	654574	4469197	920	San Blas
8463O	686070	4445844	981	Sarrión
9358G	612523	4543801	1090	Torralba de los Frailes
8489A	732768	4479473	1131	Villafranca del Cid
9358I	609067	4546895	990	Aldehuela de Liestos
3003B	592776	4494424	1192	Peralejo de las Truchas
9372	644930	4479802	1023	Cella
9375C	643663	4495001	980	Torremocha del Jiloca

References

EEA. 2007. CLC2006 technical guidelines. EEA Technical Report No 17. Copenhagen: European Environmental Agency (EEA).

IGME. 2012. Mapa geológico de España a escala 1:50,000. Cartografía Geológica Digital Magna. Madrid: Instituto Geológico y Minero de España (IGME).

Longares-Aladren LA, Mateo-Sanz G. 2014. La vegetación de la provincia de Teruel. Teruel: Instituto de Estudios Turolenses.

Ninyerola M, Pons X, Roure JM. 2005. Atlas climático digital de la Península Ibérica. Metodología y aplicaciones en bioclimatología y geobotánica. Bellaterra: Universidad Autónoma de Barcelona.

Trabucco A, Zomer RJ. 2009. Global potential evapo-transpiration (Global-PET) dataset. Consortium of International Agricultural Research Centers (CGIAR), Consortium for Spatial Information (CSI). Published online, available from the CGIAR-CSI Geoportal at www.cgiar-csi.org.

Appendix B: This appendix contains a complementary analysis on the influence of site distance to the nearest human settlements (as a proxy of human disturbance) and landscape geomorphology on the spatial variations of vegetation condition for our study sites

Objective of analysis:

The objective of this complementary analysis was to test for the assumption that disturbance intensity as it is measured in this study is a consequence of local deforestation by human activities (i.e. agriculture, livestock and fuel wood consumption) typically nucleated in the proximity of the villages, and is not a consequence of other environmental factors linked to site geomorphology (i.e. hillslope gradient and aspect).

Data sources for analysis:

We quantified site distances to the nearest human settlements (i.e. rural towns and hamlets) in the region by applying GIS spatial analysis. Those distances were further used as a proxy of human influence for the analysis of tree cover patterns in our sites. Geomorphological information (i.e. mean slope gradient and aspect) for each study site was obtained from the Digital Elevation Model MDT25 (25 m resolution, mean square error 50 cm) developed with LiDAR technologies within the Spanish National Plan for Earth Observation (PNOA) and distributed by the Spanish National Geographic Institute (IGN). Tree cover values were determined by applying supervised classification to recent high-resolution (50 cm) digital orthophotos (details in the methods of the paper).

Statistical methods:

We applied a linear mixed model (LMM) with slope angle (º), aspect (º), and site distance to the nearest human settlement (D_{Hs}, km) as continuous (fixed) predictors for tree cover (TC, %). Human settlement was applied as a random variable in the LMM to account for pattern variations between different towns/villages. Site aspect was cosine-transformed, taking values ranging from 1 to -1 for North and South aspect, respectively.

Results and Discussion:

Neither slope angle ($F_{1, 122}=2.76$, $P=0.10$) nor aspect ($F_{1, 122}=0.54$, $P=0.46$) showed significant effects on tree cover for our study sites. Site distance to the nearest human settlement significantly impacted site vegetation conditions ($F_{1, 122}=5.65$, $P=0.02$), by increasing tree cover (fixed-term slope 5.21±2.19). A good example of this effect is illustrated by the group of sites located in the vicinity of Santa Eulalia, within the valley of the Jiloca River (Fig. B1a). Tree cover strongly increased with site distance from the town center (Fig. B1b). This effect responds to the traditional patterns of land use in rural

settlements for important areas of the Iberian Peninsula and the Mediterranean basin (Grove and Rackham 2001, Millington and others 2008, Barton and others 2010), where human activities (i.e. agriculture, livestock and fuel wood consumption) are typically concentrated in the proximity of the villages. Overall, these results indicated a major role of site distance to the human settlements for organizing tree cover in our study sites, pointing out that variations of tree cover within each town vicinity reflect local intensity levels of human disturbance.
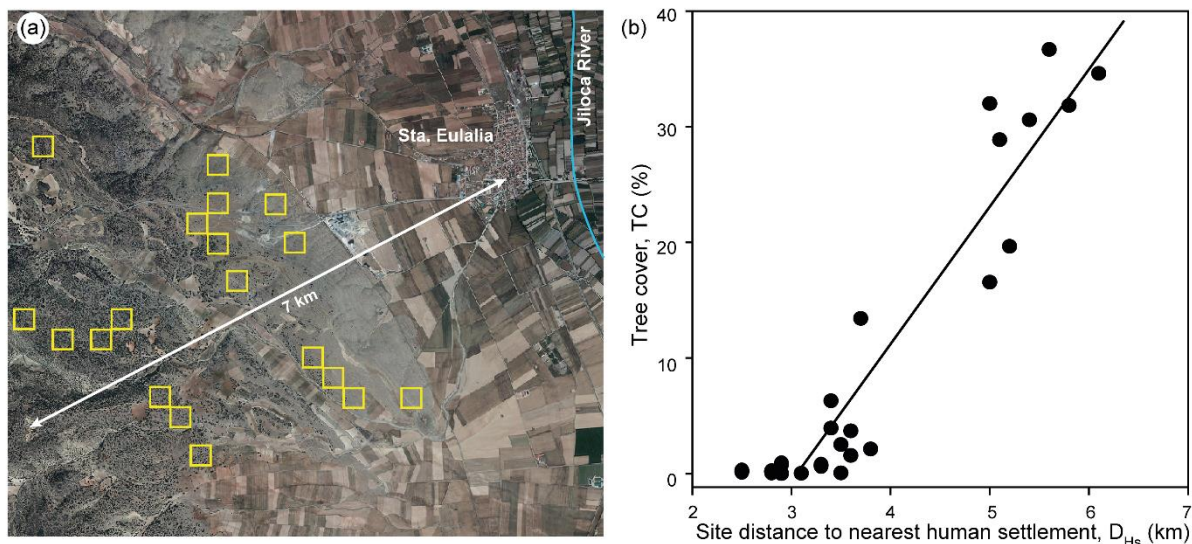

Figure B1. Impact of site distance to the closest human settlement (D_{Hs}, km) on tree cover (TC, %) for 19 sites located nearby Santa Eulalia (Jiloca River valley): (a) site locations; (b) relation between tree cover and site distance to the town center. The yellow frames in (a) indicate the 19 sites (each 231 x 231 m). Source for background image in (a): 2012 PNOA aerial picture (IBERPIX platform, http://www.ign.es/iberpix2/visor/).

References

Barton CM, Ullah II, Bergin S. 2010. Land use, water and Mediterranean landscapes: modelling long-term dynamics of complex socio-ecological systems. Philos Trans R Soc A-Math Phys Eng Sci 368:5275-97.

Grove AT, Rackham O. 2001. The nature of Mediterranean Europe: an ecological history. New Haven: Yale University Press.

Millington J, Romero-Calcerrada R, Wainwright J, Perry G. 2008. An agent-based model of Mediterranean agricultural land-use/cover change for examining wildfire risk. JASSS J Artif Soc S 11:4. http://jasss.soc.surrey.ac.uk/11/4/4.html.

Appendix C: This appendix contains an extended description of the methods for data analysis, including fully explicit equations for the modelled PUE-Dl relationships

Our data analysis methods were built on the hypothesis that aridity largely influences the response of vegetation PUE to human disturbance for our 138 study Iberian holm oak landscapes, with the less arid, sub-humid extreme of the gradient showing linear reductions of landscape functionality with disturbance (Fig. C1, degradation trend 1), and the semi-arid extreme showing accelerated, non-linear loss of ecosystem function (Fig. C1, degradation trend 2).
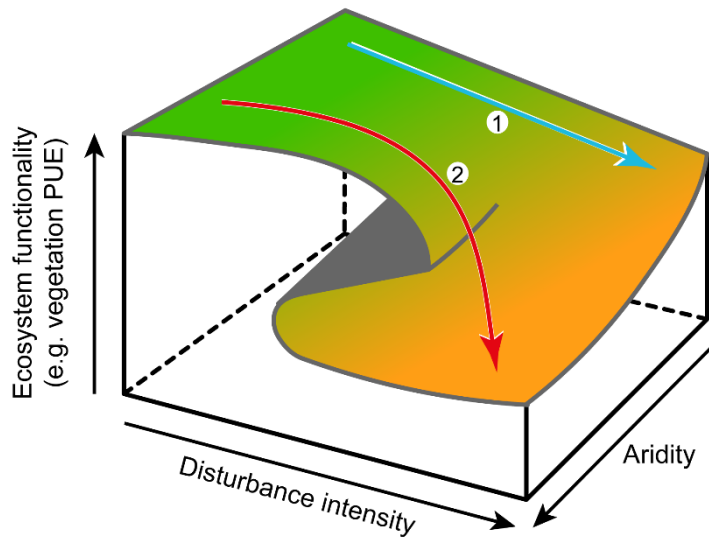

Figure C1. Conceptual model summarizing the effects of disturbance and aridity on ecosystem functionality: (1) hypothesized linear response for sub-humid conditions; (2) hypothesized accelerated, non-linear response for semi-arid conditions.

The relationship between precipitation-use efficiency (PUE) and disturbance intensity (as described by the local deforestation level, Dl) for our holm oak sites was modelled to fit a quadratic function, allowing for separate, specific relationships for each climate aridity type (semi-arid, dry-transition and sub-humid). We averaged the PUE values over the 14 hydrological years to model the mean trend, yielding a single value for each of the 138 sites. We fitted the following model:

$$E(PUE) = \beta_0 + \beta_1 I_{SA} + \beta_2 I_{DT} + \beta_3 Dl + \beta_4 Dl^2 + \beta_5 I_{SA} Dl + \beta_6 I_{DT} Dl + \beta_7 I_{SA} Dl^2 + \beta_8 I_{DT} Dl^2$$

(equation C1),

where $E(PUE)$ is the mean precipitation use efficiency (10^{-2} mm^{-1}); I_{SA} is a dummy indicator variable for the semi-arid climate type (I_{SA}=1 if the site is under semi-arid climate and 0 otherwise); I_{DT} is an indicator variable of the dry-transition climate type (I_{DT}=1 if the site is under dry-transition climate and 0 otherwise); Dl is the disturbance intensity index; and β_0 through β_8 are parameters to be estimated.

The null hypothesis that the quadratic term was the same for the three climate types was rejected (H_0: $\beta_7 = \beta_8 = 0$, P=0.048, F=3.1 on 2 and 128 d.f.), indicating that each climate type required separate quadratic functions. The (intercept, linear and quadratic term) coefficients (as well as their standard

errors) of the separate functions were estimated as linear combinations of the β parameters from the overall model (equation C1), given the following model structure for each climate type:

Sub-humid conditions:

$$E(PUE \mid I_{SA} = 0, \ I_{DT} = 0) = \beta_0 + \beta_3 Dl + \beta_4 Dl^2 \qquad \text{(equation C2)},$$

Dry-transition conditions:

$$E(PUE \mid I_{SA} = 0, \ I_{DT} = 1) = (\beta_0 + \beta_2) + (\beta_3 + \beta_6) Dl + (\beta_4 + \beta_8) Dl^2 \qquad \text{(equation C3)},$$

Semi-arid conditions:

$$E(PUE \mid I_{SA} = 1, \ I_{DT} = 0) = (\beta_0 + \beta_1) + (\beta_3 + \beta_5) Dl + (\beta_4 + \beta_7) Dl^2 \qquad \text{(equation C4)}.$$

We extended equation C1 to account for the influence of the type of hydrological year (dry *versus* wet years along the study period) on the PUE-Dl relationship. We averaged the values of PUE for dry (wet) years with below-average (above-average) precipitation of the 1998-2014 series and extended the model by adding a dummy indicator variable for type of year as well as all its interactions with climate aridity type and the linear and quadratic terms of the function, totaling 9 additional parameters. In addition, the model included a random effect for site to account for the lack of independence between dry and wet observations from the same site, given the following structure:

$$PUE_{ij} = \beta_0 + \beta_1 I_{SA_{ij}} + \beta_2 I_{DT_{ij}} + \beta_3 I_{Dry_{ij}} + \beta_4 Dl_{ij} + \beta_5 Dl_{ij}^2 + \beta_6 I_{SA_{ij}} I_{Dry_{ij}} + \beta_7 I_{DT_{ij}} I_{Dry_{ij}} +$$

$$\beta_8 I_{SA_{ij}} Dl_{ij} + \beta_9 I_{DT_{ij}} Dl_{ij} + \beta_{10} I_{SA_{ij}} Dl_{ij}^2 + \beta_{11} I_{DT_{ij}} Dl_{ij}^2 + \beta_{12} I_{Dry_{ij}} Dl_{ij} + \beta_{13} I_{Dry_{ij}} Dl_{ij}^2 +$$

$$\beta_{14} I_{SA_{ij}} I_{Dry_{ij}} Dl_{ij} + \beta_{15} I_{DT_{ij}} I_{Dry_{ij}} Dl_{ij} + \beta_{16} I_{SA_{ij}} I_{Dry_{ij}} Dl_{ij}^2 + \beta_{17} I_{DT_{ij}} I_{Dry_{ij}} Dl_{ij}^2 + u_i + e_{ij}$$

$$\text{(equation C5)},$$

where the subindex i denotes the site and j whether the observation corresponds to the wet or dry year average; *PUE* represents the precipitation-use efficiency value (10^{-2} mm^{-1}); I_{SAij} and I_{DTij} are the dummy indicator variables for the semi-arid and dry-transition climate types, respectively; Dl_{ij} is the local deforestation level of the sites; $I_{Dry \ ij}$ is the dummy indicator variable for dry hydrological year (I_{Dry}=1 for dry and 0 for wet); u_i is the site random effect component; and e_{ij} is the residual error.

The number of dry years was different among sites, ranging between 4 and 6 (out of 14), and so the PUE averages for modelling the mean PUE-Dl trends were based on different sample sizes for each site and type of hydrological year. Thus, we fitted a weighted model, with weights proportional to the number of observations used to compute the average responses. The null hypothesis that the quadratic term was the same for the two types of hydrological year was rejected (P=0.015, F=4.3 on 2 and 137 d.f.), indicating that each combination of climate and hydrological year type required separate quadratic functions. We estimated the (intercept, linear and quadratic term) coefficients (as well as their standard errors) of the separate functions as linear combinations of the parameters from the

extended model (equation C5), given the following mean trend structure for each combination of climate and hydrological year type:

Sub-humid conditions, wet year:

$$E\big(PUE \mid I_{SA} = 0,\ I_{DT} = 0,\ I_{Dry} = 0\big) = \beta_0 + \beta_4 Dl + \beta_5 Dl^2 \quad \text{(equation C6)},$$

Sub-humid conditions, dry year:

$$E\big(PUE \mid I_{SA} = 0,\ I_{DT} = 0,\ I_{Dry} = 1\big) = (\beta_0 + \beta_3) + (\beta_4 + \beta_{12})Dl + (\beta_5 + \beta_{13})Dl^2 \quad \text{(equation C7)},$$

Dry-transition conditions, wet year:

$$E\big(PUE \mid I_{SA} = 0,\ I_{DT} = 1,\ I_{Dry} = 0\big) = (\beta_0 + \beta_2) + (\beta_4 + \beta_9)Dl + (\beta_5 + \beta_{11})Dl^2 \quad \text{(equation C8)},$$

Dry-transition conditions, dry year:

$$E\big(PUE \mid I_{SA} = 0,\ I_{DT} = 1,\ I_{Dry} = 1\big) = (\beta_0 + \beta_2 + \beta_3 + \beta_7) + (\beta_4 + \beta_9 + \beta_{12} + \beta_{15})Dl +$$
$$(\beta_5 + \beta_{11} + \beta_{13} + \beta_{17})Dl^2 \quad \text{(equation C9)},$$

Semi-arid conditions, wet year:

$$E\big(PUE \mid I_{SA} = 1,\ I_{DT} = 0,\ I_{Dry} = 0\big) = (\beta_0 + \beta_1) + (\beta_4 + \beta_8)Dl + (\beta_5 + \beta_{10})Dl^2 \quad \text{(equation C10)},$$

Semi-arid conditions, dry year:

$$E\big(PUE \mid I_{SA} = 1,\ I_{DT} = 0,\ I_{Dry} = 1\big) = (\beta_0 + \beta_1 + \beta_3 + \beta_6) + (\beta_4 + \beta_8 + \beta_{12} + \beta_{14})Dl +$$
$$(\beta_5 + \beta_{10} + \beta_{13} + \beta_{16})Dl^2 \quad \text{(equation C11)}.$$

Goodness of fit for the general PUE-Dl model (equation C1) was assessed using the coefficient of determination (R^2). Similarly, marginal and conditional R^2 were calculated for the extended PUE-Dl model with mixed-effect structure (equation C5).

Variations in the explored ecosystem degradation trends were assessed by evaluating the size (absolute values) and statistical significance of the coefficients for the separate PUE-Dl functions. Particularly, statistical significance for the quadratic terms in the modelled separate PUE-Dl functions provided evidence for the occurrence of non-linear, accelerated loss of ecosystem functionality in response to the effect of disturbance. Furthermore, the size of the quadratic terms in the separate PUE-Dl functions was used to evaluate the abruptness (or curvature) of the studied ecosystem degradation trends.